

# CNN Explainability with Multivector Tucker Saliency Maps for Self-Supervised Models

**Aymene Mohammed Bouayed**

*DIÉNS, ÉNS, CNRS, PSL University, Paris, France  
Be-Ys Research, France*

*aymene.bouayed@ens.fr*

**Samuel Deslauriers-Gauthier**

*Centre Inria d'Université Côte d'Azur, Nice, France*

*samuel.deslauriers-gauthier@inria.fr*

**Adrian Iaccovelli**

*Be-Ys Research, France*

*adrian.iaccovelli@be-ys.com*

**David Naccache**

*DIÉNS, ÉNS, CNRS, PSL University, Paris, France*

*david.naccache@gmail.com*

## Abstract

Interpreting the decisions of Convolutional Neural Networks (CNNs) is essential for understanding their behavior, yet explainability remains a significant challenge, particularly for self-supervised models. Most existing methods for generating saliency maps rely on ground truth labels, restricting their use to supervised tasks. EigenCAM is the only notable label-independent alternative, leveraging Singular Value Decomposition to generate saliency maps applicable across CNN models, but it does not fully exploit the tensorial structure of feature maps. In this work, we introduce the Tucker Saliency Map (TSM) method, which applies Tucker tensor decomposition to better capture the inherent structure of feature maps, producing more accurate singular vectors and values. These are used to generate high-fidelity saliency maps, effectively highlighting objects of interest in the input. We further extend EigenCAM and TSM into multivector variants—Multivec-EigenCAM and Multivector Tucker Saliency Maps (MTSM)—which utilize all singular vectors and values, further improving saliency map quality. Quantitative evaluations on supervised classification models demonstrate that TSM, Multivec-EigenCAM, and MTSM achieve competitive performance with label-dependent methods. Moreover, TSM enhances explainability by approximately 50% over EigenCAM for both supervised and self-supervised models. Multivec-EigenCAM and MTSM further advance state-of-the-art explainability performance on self-supervised models, with MTSM achieving the best results.

## 1 Introduction

Convolutional Neural Networks (CNNs) demonstrate exceptional performance across various computer vision applications (Redmon et al., 2016; Krizhevsky et al., 2017; Liu et al., 2021). These networks can be trained in a supervised manner to tackle classification or regression tasks (He et al., 2016) or in a self-supervised manner for image segmentation (Walsh et al., 2022; Kirillov et al., 2023), face recognition (Boutros et al., 2022), and learning image embeddings (Bardes et al., 2022). However, their inherent black-box nature poses significant challenges, particularly in medicine (Cruciani et al., 2021; Bouayed et al., 2022) and biometrics (Kim & Cho, 2021), where explainability is crucial for trust and adoption.

Numerous works have attempted to address the challenge of explaining CNN decisions, proposing diverse methods that can be broadly categorized into feature attribution methods and Class Activation Map (CAM) methods. Feature attribution methods involve either estimating a locally interpretable model (Ribeiro et al.,

2016) or propagating information from the network’s output to its input using gradients (Springenberg et al., 2015), contribution scores (Bach et al., 2015; Shrikumar et al., 2017), or Shapley values (Lundberg & Lee, 2017). However, these methods often come with significant computational overhead, even when using approximations (Aas et al., 2021). In contrast, CAM methods (Zhou et al., 2016; Chattopadhyay et al., 2018) perform a weighted sum of the feature map tensors and avoid backward propagation, yet they still rely on ground truth information to infer the weights (Chattopadhyay et al., 2018; Wang et al., 2020; Desai & Ramaswamy, 2020; Schulz et al., 2020; Zhang et al., 2024).

Despite these advancements, a major limitation of current explainability methods is their predominant focus on supervised classification models. Most existing techniques rely heavily on ground truth labels to generate saliency maps, rendering them label-dependent and restricting their applicability to supervised tasks. The only exception is EigenCAM (Muhammad & Yeasin, 2020), which offers a label-independent approach and can be applied to both supervised and self-supervised models. However, EigenCAM has notable drawbacks: its use of matricization<sup>1</sup> disrupts the spatial relationships within the feature maps, particularly in the height and width dimensions. This limitation leads to less accurate estimations of singular vectors and negatively impacts the quality of the resulting saliency maps.

In this work, we aim to propose a general label-independent explainability method for CNNs that addresses the limitations of existing approaches, particularly EigenCAM. Specifically, we seek to answer the question: "*Can tensor algebra provide a better estimation of the weight vector?*". We answer the question positively through the introduction of the *Tucker Saliency Map* (TSM) method. TSM applies Tucker tensor decomposition (Kolda & Bader, 2009; Cheng et al., 2023) directly to the feature map tensor, preserving spatial relationships and resulting in different singular vectors. This enhancement allows for improved saliency maps that capture more variance in the first singular vector.

Furthermore, we extend both EigenCAM and TSM into multivector variants: *Multivec-EigenCAM* and *Multivector Tucker Saliency Maps* (MTSM), which leverage all singular vectors and values to create richer and more accurate saliency maps than their respective base methods.

We evaluate our proposed methods in both label-dependent and label-independent settings. In the label-dependent context, TSM, Multivec-EigenCAM, and MTSM demonstrate competitive performance against six state-of-the-art label-dependent CAM methods while showing substantial improvements over EigenCAM. For the label-independent setting, we introduce a comprehensive evaluation framework tailored for self-supervised models, addressing a significant gap in the literature. This framework assesses the impact of saliency maps on downstream classification performance, the reproducibility of generated embeddings, and their similarity to ground truth segmentation maps. Our results consistently show that TSM outperforms EigenCAM, establishing a new state-of-the-art in self-supervised CNN explainability. Multivec-EigenCAM and MTSM further enhance these results, particularly with MTSM leading in performance.

We outline our contributions as follows :

- We introduce Tucker Saliency Map (TSM) for label-independent CNN explainability, leveraging Tucker tensor decomposition to enhance saliency map quality.
- We develop Multivec-EigenCAM and Multivector Tucker Saliency Maps (MTSM) to utilize all singular vectors for richer saliency maps.
- We introduce a new framework for assessing saliency maps in self-supervised models, focusing on classification performance, embedding reproducibility and alignment with segmentation masks.
- We evaluate the proposed methods in both label-dependent and label-independent settings, showing competitive performance against state-of-the-art methods. Also, we establish TSM as a new state-of-the-art in self-supervised explainability, with MTSM furthering the state-of-the-art performance.

The remained of this paper is organized as follows: in Section 2 introduces essential background definitions and notations. Section 3 reviews related work addressing various explainability methods for CNN models. The mechanics of our proposed methods are detailed in Sections 4 and 5. We rigorously test and verify

<sup>1</sup>Matricization is the operation of transforming a tensor into a matrix (Kolda & Bader, 2009).

the efficacy of our methods across a diverse set of supervised and self-supervised CNN models in Section 6. Finally, we conclude and outline potential avenues for future exploration in Section 7.

## 2 Background

### 2.1 Class Activation Maps

Class Activation Maps (CAMs) (Zhou et al., 2016) are local explainability methods for CNN based models. They help visualize the regions of the input image that significantly contribute to the CNN’s prediction by analyzing the intermediate results. Formally, CAMs are defined as the sum of the feature maps resulting from the last convolutional layer of a CNN  $\mathcal{F} \in \mathbb{R}^{C,H,W}$ , weighted by a vector  $w \in \mathbb{R}^C$  as follows:

$$\text{CAM} = \sum_{i=1}^C w_i \mathcal{F}_i. \quad (1)$$

As observed from Equation 1, the weight vector  $w$  is the only unknown to determine<sup>2</sup>. Various works propose different methods to infer  $w$  (Chattopadhyay et al., 2018; Wang et al., 2020; Muhammad & Yeasin, 2020; Zhang et al., 2024). In Section 3.2, we provide an overview of the different CAM based methods with a focus on the EigenCAM method (Muhammad & Yeasin, 2020) which utilizes the SVD (Trefethen & Bau, 1997).

### 2.2 Matrix Decomposition and SVD

Matrix decomposition involves factorizing a matrix  $\mathcal{M} \in \mathbb{R}^{m,n}$  into a product of  $k$  matrices to simplify computations and reveal underlying structures (Trefethen & Bau, 1997). Singular Value Decomposition (SVD) (Trefethen & Bau, 1997) is a prominent matrix decomposition method, which expresses a matrix  $\mathcal{M}$  as  $\mathcal{M} = U\Sigma V^\top$ . Matrices  $U \in \mathbb{R}^{m,m}$  and  $V \in \mathbb{R}^{n,n}$  consist of *singular vectors* and form a basis for the rows and columns of  $\mathcal{M}$ , respectively. The matrix  $\Sigma \in \mathbb{R}^{m,n}$  is a diagonal matrix containing *singular values* on the diagonal, representing the information and variance encoded per direction of the new basis (Trefethen & Bau, 1997). However, the SVD is exclusively applicable to matrices therefore can not be applicable to higher dimensional data in the form of tensors without the need to undergo a matricization operation. This ultimately results in a loss of relationship information between the elements of flattened modes. Consequently, tensor algebra introduces a multitude of decompositions which operate directly in the tensor space hence solving the relationship disruption problem.

### 2.3 Tensors and Tucker Decomposition

A tensor  $\mathcal{T} \in \mathbb{R}^{n_1, n_2, \dots, n_k}$  an algebraic object that can be thought of as a multi-dimensional array that generalizes matrices to higher dimensions, allowing for more complex data representations. Consequently, a multitude of operations on matrices can be extended to tensors. One such extension is *tensor decomposition* (Kolda & Bader, 2009). Among the most well known tensor decompositions we find the *CANDECOMP/PARAFAC* (CP) decomposition (Kiers, 2000; Bove, 2010) and the *Tucker tensor decomposition* (Sheehan & Saad, 2007; Cheng et al., 2023). As noticed by Kolda & Bader (2009), CP decomposes a tensor as a sum of rank-one tensors with no additional constraints, whereas the Tucker tensor decomposition is a higher-order form of principal component analysis. Hence, the Tucker decomposition provides sorted singular vectors according to singular values as opposed to the CP decomposition. This property is of importance to the modeling of our proposed TSM methods and motivates our choice of the Tucker decomposition over the CP decomposition or any other decomposition (See Section 4).

Focusing on the Tucker tensor decomposition, it decomposes a tensor  $\mathcal{T}$  as :

$$\mathcal{T} = \mathcal{C} \times_1 A^{(1)} \times_2 A^{(2)} \times_3 \dots \times_k A^{(k)}. \quad (2)$$

<sup>2</sup>Additional operations can be applied to the weighted sum depending on the CAM method. Among such operations is the ReLU function and/or the min-max normalization.

Here,  $\mathcal{C} \in \mathbb{R}^{n_1, n_2, \dots, n_k}$  is the core tensor containing singular values calculated by taking the Frobenius norm along each mode  $i$ . The symbol  $\times_i$  denotes matrix multiplication along the  $i^{\text{th}}$  mode, and  $A^{(1)}, \dots, A^{(k)}$  are unitary matrices representing the newly calculated basis, akin to the matrices  $U$  and  $V$  in SVD.

The estimation of the values of the core tensor  $\mathcal{C}$  and the basis  $\{A^{(i)}\}_{i=1}^k$  can be achieved through different algorithms, notably, the Higher Order Orthogonal Iteration (HOOI) algorithm (Sheehan & Saad, 2007) or the Higher-Order SVD (HOSVD) (De Lathauwer et al., 2000) algorithm. In this work, we harness the HOOI algorithm, as it is known to be more accurate than HOSVD for Tucker Decomposition. HOOI uses HOSVD as an initialization step increasing the chances of having a unique solution which is then optimized in order to minimize the the Frobenius form between the tensor  $\mathcal{T}$  and its decomposition (Kolda & Bader, 2009).

### 3 Related work

#### 3.1 Feature attribution methods

Feature attribution methods are explainability techniques which assign a weight to each feature of the input, such as a pixel in an image (Lundberg & Lee, 2017). One such feature attribution method is the *Guided Backpropagation* method (Springenberg et al., 2015), which propagates positive gradients of the classification loss function to the input. However, to address the gradient saturation and the stochastic nature of gradients, methods like *Layer-wise Relevance Propagation (LRP)* (Bach et al., 2015) and DeepLFT (Shrikumar et al., 2017) were proposed. These methods calculate a relevance score for the output of each neuron  $j$  as a weighted sum of all the neurons it is connected to. This operation is then back-propagated till the input, resulting in a heatmap showcasing the importance of each region to the network’s output (Montavon et al., 2019). However, Lundberg & Lee (2017) notices that the latter methods require domain-specific knowledge, which is dataset-specific, and therefore introduces *Deep SHapley Additive exPlanations (Deep SHAP)* (Lundberg & Lee, 2017). Deep SHAP uses Shapley values (Ichiishi, 1983) to calculate the contribution of each feature in the network’s input. Despite its strong theoretical backing, Deep SHAP’s computational complexity poses challenges for large datasets, making it less practical for real-time applications, even with approximation methods (Aas et al., 2021). Moreover, all the stated methods highlights certain pixels which does not produce spatially human-interpretable coherent maps. LIME (Ribeiro et al., 2016) solves the latter problem and highlights contiguous regions of the input. This is achieved by perturbing input data and create a locally interpretable model around the predicted classification, relying on the model’s output class.

All feature attribution methods are inherently label-dependent, as they calculate saliency maps based on a specified target class in different ways. The reliance of feature attribution methods on label information prevents their application to self-supervised models, where no ground truth labels are available. In contrast, our proposed methods, TSM and MTSM, operate in a label-independent manner and produce visually interpretable saliency maps by highlighting larger, contiguous regions of the input. Consequently, in our experiments we exclusively evaluate the performance of feature attribution methods on classification models.

#### 3.2 Class activation map methods

Building on feature attribution techniques, Class Activation Maps (CAMs) (Zhou et al., 2016) offer a visual interpretation of model predictions, particularly in computer vision tasks. They have also found application in different domains, such as anomaly detection (Kimura et al., 2020), disease identification and localization (Khan et al., 2019; Bouayed et al., 2022). CAM methods can be broadly categorized into *label-dependent* and *label-independent* methods. Below is a brief description of each family of CAMs.

##### 3.2.1 Label-dependent class activation maps

Label-dependent class activation maps rely on the label information associated with the input. This label information is combined with the output of the network to estimate a loss and backpropagate the loss information to infer the weight vector  $w$ . This information can be in the form of gradients as in GradCAM (Selvaraju et al., 2017) and XGradCAM (Fu et al., 2020), or the impact of each feature map on the correct classification as in ScoreCAM (Wang et al., 2020) and AblationCAM (Desai & Ramaswamy,



2020). Other methods perform an optimization procedure on  $w$  to minimize the model’s training loss namely Information Bottleneck Attribution (Schulz et al., 2020) and Opti-CAM (Zhang et al., 2024).

These methods primarily target classification models, providing explanations based on the assumption that the class with the highest probability is the true class. This assumption depends heavily on the performance of the model and that no out of distribution data is used. Additionally, the most widely used label depend methods are gradient methods such as GradCAM (Selvaraju et al., 2017) however gradient information is inherently noisy.

Recent work (Ramprasaath R. Selvaraju, 2021; Shu et al., 2023) use the gradient of the contrastive loss to calculate the GradCAM based saliency map of a self-supervised model. However, such loss heavily depends on the batch size and the type of transformation used, in addition to the gradient instability, this would results in saliency maps which depend on multiple factors. As a result, in our experiments we only consider label-depend methods on classification models.

### 3.2.2 Label-independent class activation maps

Label-independent class activation maps rely on the decomposition of the feature map tensor to infer the weight vector  $w$ . To the best of our knowledge, EigenCAM (Muhammad & Yeasin, 2020) is the only method in this family. EigenCAM flattenes the feature map tensor into a matrix, and after applying the SVD (Trefethen & Bau, 1997), the first right singular vector is used as the weight vector. Despite EigenCAM’s good performance, the matricization step disrupts spatial relationships between dimensions, captures a limited amount of variance in the first singular vector and fails to utilize the full potential of tensor algebra, leading to a less accurate weight vector and a lower quality saliency map. To address these shortcomings, in the following Section 4 we propose the TSM method, which leverages Tucker tensor decomposition for more accurate weight vector estimation and improved saliency maps. Moreover, since both EigenCAM and TSM rely only on one singular vector, in Section 5 we propose an extension of both methods to harness all the singular vectors and singular values.

## 4 Tucker Saliency Maps

The Tucker Saliency Map (TSM) method is a local explainability approach. It involves generating saliency maps in the form of heat maps highlighting significant regions in the input images of a CNN related to the task at hand. To accomplish this, firstly the feature map tensor outputted by a convolutional layer is retrieved. Then, a weighted sum of this tensor is performed along the channels mode with the weight vector weighting each feature map estimated through the Tucker tensor decomposition. Consequently, it can be noticed that TSM is applicable to both supervised and self-supervised CNN models as it does not require information regarding the loss but only requires access to the feature map tensor. Figure 1 provides an overview of the proposed method, visually summarizing its key components and process.

In detail, given a feature map tensor  $\mathcal{F} \in \mathbb{R}^{C,H,W}$  retrieved as the output of a convolutional layer, we firstly perform its Tucker tensor decomposition :

$$\mathcal{F} = \mathcal{C} \times_1 A^{(1)} \times_2 A^{(2)} \times_3 A^{(3)} \quad (3)$$

With  $\mathcal{C}$  being the core tensor,  $A^{(1)} \in \mathbb{R}^{C,C}$ ,  $A^{(2)} \in \mathbb{R}^{H,H}$ , and  $A^{(3)} \in \mathbb{R}^{W,W}$  are the matrices containing the orthonormal singular vectors for each dimension. The choice of Tucker tensor decomposition among all tensor decomposition methods is strategic, as it accurately identifies the direction of highest variance, a feature crucial for weighting feature maps effectively (Kolda & Bader, 2009).

Secondly, inspired by the work of Muhammad & Yeasin (2020), we consider the first singular vector i.e. the one associated to the largest singular value,  $A_1^{(1)}$  of the matrix  $A^{(1)}$  as the weight vector  $w \in \mathbb{R}^C$ . This can be seen as projecting the feature map tensor on the direction with the highest variance. As a result, the obtained saliency maps highlighting more of the regions important to the model’s output hence more accurate

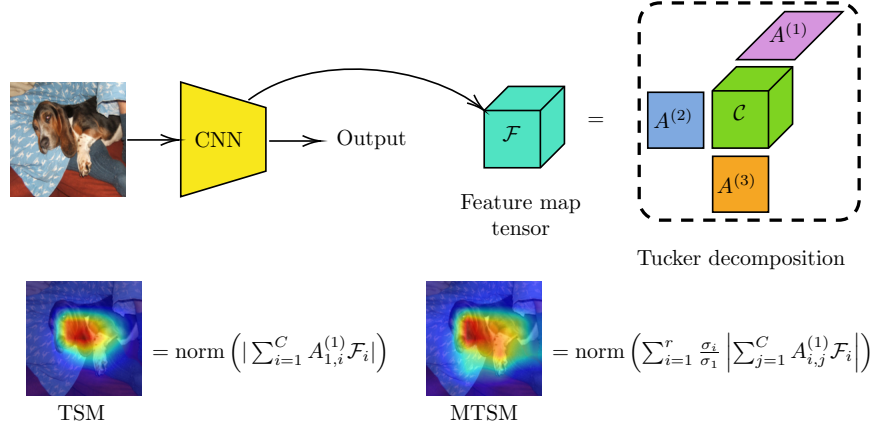


Figure 1: Proposed TSM and MTSM methods. Firstly, the feature map tensor  $\mathcal{F}$  is extracted from the output of a convolutional layer (preferably the last convolutional layer, as it has the widest field of view). Then, the Tucker tensor decomposition (Sheehan & Saad, 2007) is performed on  $\mathcal{F}$ . This decomposition results in a core tensor  $\mathcal{C}$  and three matrices containing orthonormal singular vectors for each dimension, notably  $A^{(1)}$ ,  $A^{(2)}$ , and  $A^{(3)}$ . The matrix  $A^{(1)}$  and the singular values are appropriately used to calculate the TSM (See Equation 4) and the MTSM (See Equation 6). Finally, the absolute value function is applied per element to the resulting matrix and the values are renormalized to be in the range  $[0; 1]$ .

local explainability. Formally, we calculate the saliency map as follows :

$$\mathcal{C}, A^{(1)}, A^{(2)}, A^{(3)} = \text{Tucker}(\mathcal{F}) \quad , \quad w = A_1^{(1)} \quad (4)$$

$$TSM = \text{norm} \left( \left| \sum_{i=1}^C w_i \cdot \mathcal{F}_i \right| \right).$$

The application of min-max normalization  $\text{norm}(\cdot)$  ensures that the saliency map's values are bounded within the  $[0, 1]$  range. The absolute value function  $|\cdot|$  is employed instead of ReLU to focus on the activation magnitude, disregarding the sign, considering the possibility of negative value multiplication in subsequent layers of the feature map  $\mathcal{F}$ .

The main difference between TSM and EigenCAM resides in the decomposition methods. EigenCAM performs an SVD decomposition after a matricization operation of the feature map tensor  $\text{mat}(\cdot)$  :

$$U, \Sigma, V^\top = \text{SVD}(\text{mat}(\mathcal{F})) \quad , \quad w = V_1. \quad (5)$$

The matricization operation on  $\mathcal{F}$  ultimately mixes the elements of the first and second mode (height and width) so as to obtain a matrix of size  $\mathbb{R}^{C, H \times W}$ . Such operation would have a negative impact on the relationships between the elements of the tensor. Therefore, performing a decomposition on such matrix results in less accurate estimation of the singular vectors and values for each mode which leads to less representative saliency maps. However, in TSM, we adopt a more general and more suitable neighborhood information preserving decomposition notably the Tucker tensor decomposition. This decomposition allows for a better approximation of the first singular vector capturing the most variance. This can be observed in Figure 2 where the amount of variance encoded by the first singular vectors using the Tucker decomposition is higher compared to the SVD decomposition on most tested models. Additionally, the use of the absolute value in the calculation of the saliency map puts forward more information hence more informative and accurate saliency maps. Nevertheless, both EigenCAM and TSM utilize only the singular vector associated with the largest singular value. In the following section, we propose a generalization of both methods to utilize all singular values and singular vectors.

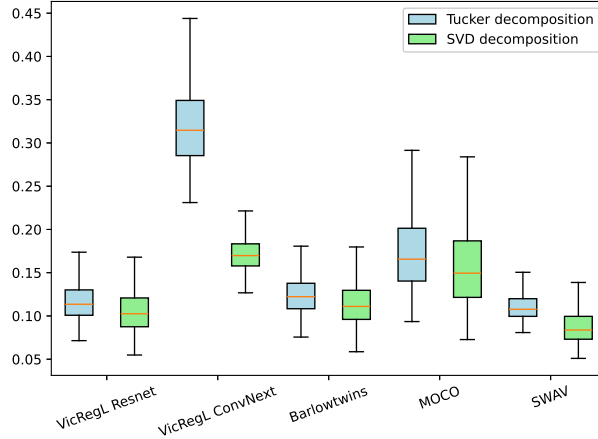


Figure 2: Boxplot comparing the distribution of the first singular values divided by the sum of all singular values per tensor in both SVD decomposition and Tucker decomposition. These singular values are obtained from the decomposition of all the feature map tensors produced by five different self-supervised models on the Pascal VOC (Everingham et al., 2010) validation dataset.

## 5 Multivector EigenCAM and Multivector Tucker Saliency Maps

Figure 3 represents the distribution of the first five singular values in both SVD decomposition and Tucker decomposition divided by the sum of all singular values per tensor. From this figure we notice that for both the SVD and Tucker decompositions singular values other than the first one encapsulate a significant amount of variance. Consequently, EigenCAM and TSM only convey a portion of the total information encoded in the feature map tensor. To this end, in this section we introduce Multivector EigenCAM and Multivector Tucker Saliency Maps (*Mutivector-EigenCAM* and *MTSM*) explainability methods. These methods generate a saliency map per singular vector in the SVD or the Tucker tensor decomposition. Then, a weighted sum of the generated saliency maps is performed. The weights of each saliency map are inferred based on the singular values such as, given  $\sigma_i$  the singular values associated with the  $i$ -th singular vector (extracted either from the SVD or the Tucker decomposition), the weight are given by  $\frac{\sigma_i}{\sigma_1}$  where  $\sigma_1$  is the largest singular value. We provide an overview of the proposed MTSM method in Figure 1.

Formally, given a feature map tensor  $\mathcal{F} \in \mathbb{R}^{C,H,W}$ , an operator  $D(\cdot)$  encapsulating the SVD or Tucker tensor decomposition and returning the ordered singular values  $\sigma \in \mathbb{R}^r$  and their corresponding singular vectors for the channels dimension  $V \in \mathbb{R}^{r,C}$ :

$$\sigma, V = D(\mathcal{F}) \tag{6}$$

$$\text{Mutivector-}^* = \text{norm} \left( \sum_{i=1}^r \frac{\sigma_i}{\sigma_1} \left| \sum_{j=1}^C V_{i,j} \mathcal{F}_i \right| \right).$$

This formulation of the Mutivector-\* can be seen as first generating the EigenCAM or TSM, since the weight of the first saliency map is one, than adding additional information to it which is generated using the rest of the singular vectors. Consequently, the produced saliency maps are richer and more precise as demonstrated quantitatively and qualitatively in Section 6.

The differentiating point between uni-vector methods to its multi-vector ones in performance would depend on the amount of variance encoded by the singular vectors other than the first one. If these vectors do not encode a large amount of variance the performance does not improve significantly (See the Tucker tensor decomposition in Figure 3(a) and the quantitative results in Table 2). However, if they encode a large amount of information, harnessing these vectors would result in significant performance improvement (See Figure 3(b)). Consequently, multi-vector saliency map methods in the worst scenario output the same result

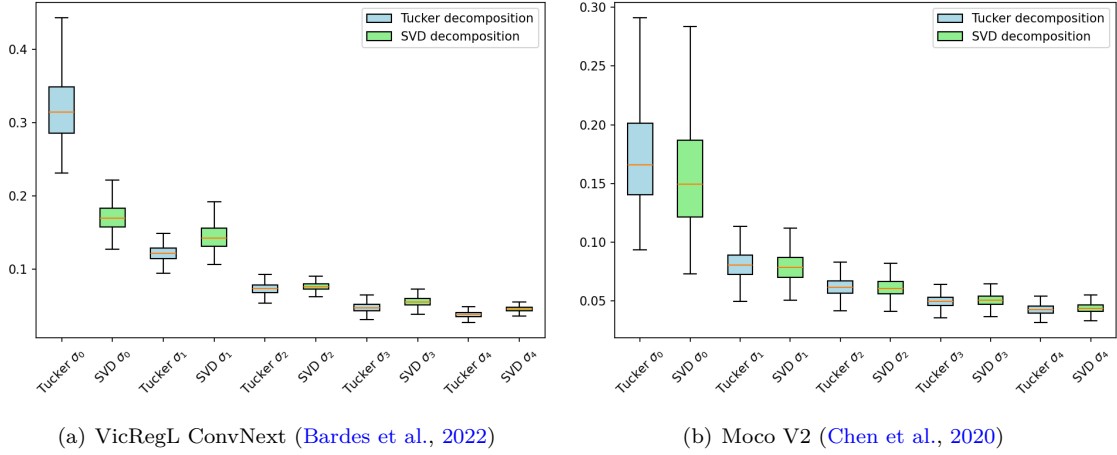


Figure 3: Boxplot representing the distribution of the first five singular values in both SVD decomposition and Tucker decomposition divided by the sum of all singular values per tensor. These singular values are obtained from the decomposition of all the feature map tensors produced by the Moco V2 (Chen et al., 2020) and VicRegL ConvNext (Bardes et al., 2022) models on the Pascal VOC validation dataset.

as the uni-vector methods. Moreover, as SVD based saliency methods do not estimate the most accurate singular vectors, we notice a significant amount of variance encoded by the rest of the singular vectors in Figure 3. Therefore, EigenCAM’s performance would greatly improve when opting for the multi-vector formulation. We quantitatively and qualitatively confirm these remarks in the following Section 6.

## 6 Experiments

In this section we start by presenting the metrics we use to evaluate explainability methods based on saliency maps both on supervised classification models and self-supervised representation learning models. Then, we present, discuss and compare the experimental results of our proposed methods compared to methods in the literature. Moreover, in Appendix A we present Python code for the implementation of our proposed methods and in Appendix B we lay out our experimental setup. Appendices D, E and F put forward additional qualitative results for the different tested supervised and self-supervised CNN models.

### 6.1 Evaluation metrics

#### 6.1.1 Supervised learning metrics

To evaluate our proposed methods on supervised models, we opt for the two conventionally used metrics, the Average Drop and Average Increase proposed in the work of Chattopadhyay et al. (2018) as they align with human interpretation and favor saliency maps with contiguous regions.

- **Average Drop (AD)** This metrics quantifies the answer to the question *"Did we hide in the image information which is relevant to the target class ?"*. To do so, the AD calculates the mean drop in classification confidence for the target class via the following formula :

$$AD(\%) = \frac{1}{N} \sum_{i=1}^N \frac{[p_i^c - o_i^c]_+}{p_i^c} \cdot 100. \quad (7)$$

- **Average Increase (AI)** This metric measures if the saliency map has removed unnecessary information from the input image, hence removing noise and improving the model’s confidence in the target

class. This is done via the following formula :

$$AI(\%) = \frac{1}{N} \sum_{i=1}^N \mathbb{I}_{p_i^c < o_i^c} \cdot 100. \quad (8)$$

In the previous formulae, we denote by  $N$  the size of the dataset and by  $c$  the ground truth label of the input  $i$ .  $p_i^c$  (respectively,  $o_i^c$ ) represents the probability of classifying the image  $i$  (respectively, the image  $i$  masked by the inferred saliency map) in class  $c$ . We note that the AD and AI metrics are to be minimized and maximized respectively.

### 6.1.2 Self-supervised learning metrics

Since, to the best of our knowledge, no framework exists for the evaluation of saliency map based explainability methods on self-supervised CNN models, we propose one. The proposed framework relies on four metrics; notably the Average Drop (AD), the Average Increase (AI) (Chattopadhyay et al., 2018), the Mean Squared Error (MSE), and the mean Intersection over Union (mIoU) metric (Jaccard, 1901).

- **Average Drop (AD) and Average Increase (AI)** (Chattopadhyay et al., 2018) To calculate the AD and AI, we estimate the saliency map from the self-supervised model, then evaluate the quality of the saliency map using pretrained supervised classification model and the formulae described in the previous Section 6.1.1. We detail the pretrained classification models used for each self-supervised model in Appendix B.4.
- **Mean Squared Error** Since self-supervised models output an encoding for each input image, we calculate the mean squared error between the encoding  $z_i$  of the image  $i$  and the encoding  $\bar{z}_i$  of the image  $i$  masked with the inferred saliency map. If the saliency map is able to isolate the important regions in the image which are encoded, there should be no difference between the encodings. This metric is to be minimized and we formulate it as follows :

$$MSE = \frac{1}{N} \sum_{i=1}^N \|z_i - \bar{z}_i\|_2^2. \quad (9)$$

- **Mean Intersection over Union** (Jaccard, 1901) Under the hypothesis that the saliency map represents a segmentation highlighting the most important parts in an image, we calculate the mean Intersection over Union segmentation metric using the ground truth segmented images in the Pascal VOC dataset (Everingham et al., 2010). Formally, we calculate this metric using the following formula :

$$B = \begin{cases} 1 & \text{if saliency\_map} \leq T \\ 0 & \text{else} \end{cases}, \quad mIoU(B, S) = \frac{|B \cap S|}{|B \cup S|}. \quad (10)$$

where  $B$  is the pixel-wise binarized saliency map according to a threshold  $T$ ,  $S$  is the ground truth binary segmentation mask and  $|B \cap S|$  (respectively,  $|B \cup S|$ ) represents the area of intersection (respectively, union) between the saliency map and the ground truth segmentation  $S$ . Moreover, to be thorough, we study the impact of the performance of the different proposed explainability methods as a function of the threshold parameter  $T$  on a multitude of models. The obtained results are reported in Appendix C. We note that this metrics is to be maximized.

## 6.2 Results and discussion on supervised classification models

We evaluate and compare the TSM, MTSM and Multivec-EigenCAM method to a multitude of saliency map extraction methods on the pretrained VGG16 (Simonyan & Zisserman, 2014), Resnet50 (He et al., 2016) and ConvNext (Liu et al., 2022) models. For the evaluation, we calculate the AD and AI on the 50,000 validation images of the ImageNet dataset. The obtained quantitative and qualitative results are presented in Table 1 and Figure 4 respectively.

Table 1: Saliency map methods comparison on the validation set of the ImageNet dataset across different pretrained classification models. The best values are highlighted in **bold**, while the second-best values are underlined. Cyan-colored rows denote label-independent saliency map methods.

Method	Resnet50		ConvNext		VGG16	
	AD(%) ↓	AI(%) ↑	AD(%) ↓	AI(%) ↑	AD(%) ↓	AI(%) ↑
GradCAM	<b>13.01</b>	<b>44.52</b>	32.49	14.67	17.58	40.32
GradCAM++	13.61	42.50	80.32	9.72	19.12	35.20
HiResCAM	<b>13.01</b>	<b>44.52</b>	32.49	<u>16.66</u>	19.18	37.59
XGradCAM	<b>13.01</b>	<b>44.52</b>	32.49	<u>16.66</u>	<u>16.00</u>	<b>41.64</b>
AblationCAM	<u>13.21</u>	43.05	51.74	10.99	17.66	38.72
OptiCAM	26.45	27.77	<b>19.60</b>	<b>26.77</b>	<b>15.59</b>	<u>40.48</u>
DeepLIFT	95.37	2.50	93.44	1.75	95.34	2.47
DeepSHAP	95.36	2.49	93.43	1.75	95.33	2.47
LIME	57.73	12.71	56.23	10.92	62.33	11.47
EigenCAM	38.51	21.41	36.24	9.69	47.32	17.11
TSM	16.86	37.27	<u>30.85</u>	9.36	26.74	27.50
Multivec-EigenCAM	22.69	30.43	37.93	9.92	25.64	27.50
MTSM	16.27	37.24	31.78	9.16	22.02	30.65

From Table 1, we notice that CAM methods’ performance is superior to that of feature attribution methods as they highlight larger contiguous regions important to the classification task. Moreover, when comparing label-dependent CAM methods to our proposed label-independent methods, we notice that the latter methods achieve competitive performance especially, on the ConvNext model where we note TSM’s second best result on the AD metric. However, label-independent methods’ performance is still lower than state-of-the-art label-dependent methods on classification models as the latter utilize more information. A fairer comparison of our proposed methods is with label-independent methods notably EigenCAM. In this setting, TSM demonstrates approximately a 50% improvement in performance across most models, measured by the AD and AI metrics. For example, on the VGG16 model, TSM achieves a 26.96% Average Drop compared to the 47.32% obtained by the EigenCAM method, representing a 56.97% improvement. Additionally, Multivec-EigenCAM and MTSM improve upon the performance of EigenCAM and TSM respectively. The magnitude of the difference in performance between uni-vector and multi-vector methods is governed by the amount of variance encoded in the singular vectors following the first one as discussed in Section 5. We perceive a larger performance jump going from EigenCAM to Multivec-EigenCAM compared to going from TSM to MTSM. This goes back to the more accurate estimation of the singular vectors by Tucker tensor decomposition and capturing of most of the variance in the first singular vector. Therefore, even though MTSM results in a smaller performance improvement gap, it significantly improves upon the performance of Multivec-EigenCAM. We further emphasize the importance of using the Tucker tensor decomposition instead of the SVD as we notice that on two out of the three tested models the uni-vector TSM achieves significantly better performance than Multivec-EigenCAM.

Figure 4 presents a qualitative comparison between a sample of label-dependent and independent methods (Additional figures are presented in Appendix D). This figure backs our quantitative results where we notice that TSM and MTSM yield saliency maps similar to the most performant label-dependent method notably GradCAM. However, the highlighted regions by TSM and MTSM can be relevant to the image class or not, showcasing the label-independent nature of the methods. This is particularly noticeable in the second image, where TSM and MTSM effectively highlights the gymnast, the public in the background, and the balance beam. Furthermore, compared to EigenCAM and Multivec-EigenCAM, TSM and MTSM highlight more of the regions in the image and with higher confidence (Notice the bedroom image in Figure 4). Finally, comparing uni-vector and multi-vector, we perceive a significant improvement of Multivec-EigenCAM over EigenCAM with more highlighted regions. Nevertheless, between TSM and MTSM little difference can be observed which joins our observation and discussion of the quantitative results.



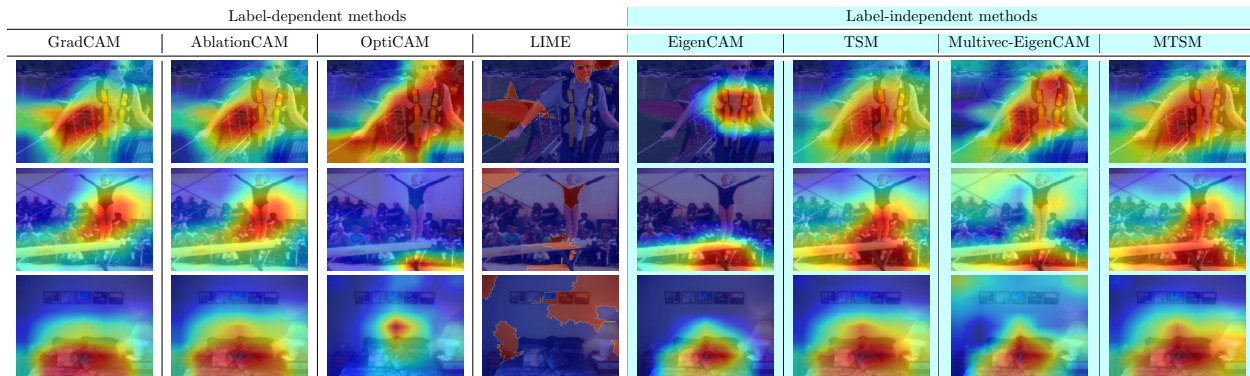


Figure 4: Qualitative comparison of saliency map-based methods on the Resnet50 model.

### 6.3 Results and discussion on self-supervised models

In this section, we present the quantitative and qualitative results obtained by the methods we propose. We analyse, discuss and compare them only to the results obtained by the EigenCAM method (Muhammad & Yeasin, 2020) as it is the only principled method which can be applied in this context<sup>3</sup>. In this section, we calculate the AD, AI and MSE metrics on the 50,000 validation images of the ImageNet dataset (Deng et al., 2009) whereas the mIoU metric is calculated on the 1,449 validation images of the Pascal VOC dataset (Everingham et al., 2010). The obtained quantitative and qualitative results are presented in Table 2 and Figures 5, and 6.

From Table 2, we observe the superior performance of Tucker decomposition based saliency map methods (i.e. TSM and MTSM) compared to the SVD based saliency map methods (i.e. EigenCAM and Multivec-EigenCAM). Additionally, similar to our observation on the supervised classification model, TSM achieves a 50% improvement in performance on all metrics compared to EigenCAM. This is attributed to the benefits of using the most suitable mathematical tools to manipulate tensors notably the Tucker tensor decomposition. Also, the use of the absolute value in the TSM and MTSM methods brings forward negative contributions which are of interest. Consequently, through the used metrics we can conclude that compared to EigenCAM, TSM is able to :

- Retain more of crucial information in the image which is relevant to image classification.
- Produce saliency maps aligned with segmentation masks.
- Conceal notably less input regions vital to the self-supervised model.

Additionally, we notice that the multi-vector methods improve on the performance of TSM. Also, Multivec-EigenCAM has a significant performance jump compared to EigenCAM as opposed to the performance gap between TSM and MTSM. This can also be explained by our previous argument on the supervised classification models which links back to the amount of variance encoded by the first singular vectors. However, for the VicRegL ConvNext model we notice a slight drop in performance going from TSM to MTSM. The reason for this is illustrated in Figure 3(a). We can see that a large portion the variance is captured by the first singular vector around 30% to 40%. Consequently, the rest of the singular values do not bring significant information. Combined with the weight assigned to these vectors, their impact on the final saliency map is minimal at best or adds noise to it.

Figures 5, and 6 qualitatively confirm the quantitative results of Table 2. These figures illustrate a superior coverage of important objects in the saliency maps generated by TSM compared to those produced by EigenCAM. For instance, we notice TSM providing better coverage of the man in the stadium and the audience behind the gymnast. Lastly, the visual representations in Figure 6 underscore the qualitative findings

<sup>3</sup>Label-dependent methods like GradCAM, which we test in the previous section, are difficult to adapt to this setting in a principled manner and can represent an interesting future work (See our discussion in Section 3.2.2).

Table 2: Comparison between TSM, EigenCAM, MTSM and Multivec-EigenCAM on self-supervised models trained on the ImageNet dataset. The reported mIoU values are computed with a threshold of 0.5 applied to the saliency maps. The best values are highlighted in **bold**.

Method	EigenCAM				TSM			
	AD(%) ↓	AI(%) ↑	MSE $\times 10^{-3}$ ↓	mIoU(%) ↑	AD(%) ↓	AI(%) ↑	MSE $\times 10^{-3}$ ↓	mIoU(%) ↑
Moco V2	38.42	32.56	0.25	23.13	<b>20.98</b>	<b>44.60</b>	<b>0.16</b>	<b>28.82</b>
SWAV	31.94	37.49	12.22	26.35	<b>14.61</b>	<b>47.23</b>	<b>5.55</b>	<b>39.97</b>
Barlow Twins	41.72	31.02	8.73	21.06	<b>21.41</b>	<b>44.69</b>	<b>5.95</b>	<b>27.91</b>
VicRegL Resnet50	42.15	30.80	75.50	21.28	<b>20.30</b>	<b>45.36</b>	<b>48.20</b>	<b>28.47</b>
VicRegL ConvNext	40.71	9.93	95.54	22.65	<b>17.42</b>	<b>13.26</b>	<b>25.57</b>	<b>36.69</b>

Method	Multivec-EigenCAM				MTSM			
	AD(%) ↓	AI(%) ↑	MSE $\times 10^{-3}$ ↓	mIoU(%) ↑	AD(%) ↓	AI(%) ↑	MSE $\times 10^{-3}$ ↓	mIoU(%) ↑
Moco V2	19.24	45.49	0.15	27.75	<b>16.38</b>	<b>46.96</b>	<b>0.12</b>	<b>33.57</b>
SWAV	16.40	44.81	6.00	37.54	<b>13.89</b>	<b>46.59</b>	<b>4.63</b>	<b>41.33</b>
Barlow Twins	18.96	45.84	5.26	32.35	<b>16.58</b>	<b>46.42</b>	<b>4.18</b>	<b>36.15</b>
VicRegL Resnet50	18.10	45.59	42.37	33.19	<b>16.30</b>	<b>46.67</b>	<b>35.98</b>	<b>35.38</b>
VicRegL ConvNext	<b>17.10</b>	15.85	31.49	26.61	17.87	<b>13.51</b>	<b>26.84</b>	<b>37.00</b>

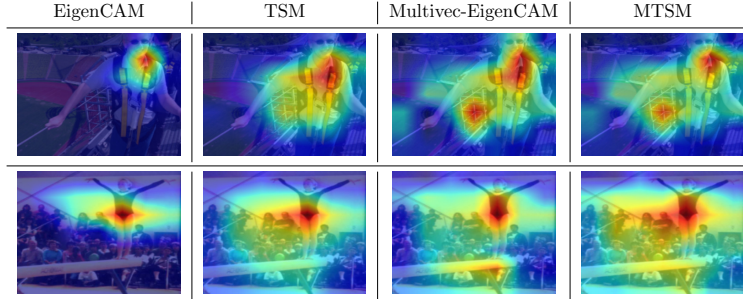


Figure 5: Qualitative comparison of saliency maps extracted using the EigenCAM versus TSM on the VicRegL Resnet50 model applied to the ImageNet dataset.

reflected in the mIoU metric of Table 2. Notably, EigenCAM (respectively Multivec-EigenCAM) highlights fewer regions of interest than TSM (respectively MTSM), leading to a lower mIoU. Moreover, in Figure 5, EigenCAM presents a substantial difference in the resulting saliency map compared to Multivec-EigenCAM whereas the latter produces saliency maps inline with those of TSM and MTSM. Consequently, EigenCAM is not able to capture all the necessary information and presents a very limited view of what the self-supervised model is focusing on. Therefore, when using EigenCAM as an explainability method the conclusion that one could arrive to might not be the correct one.

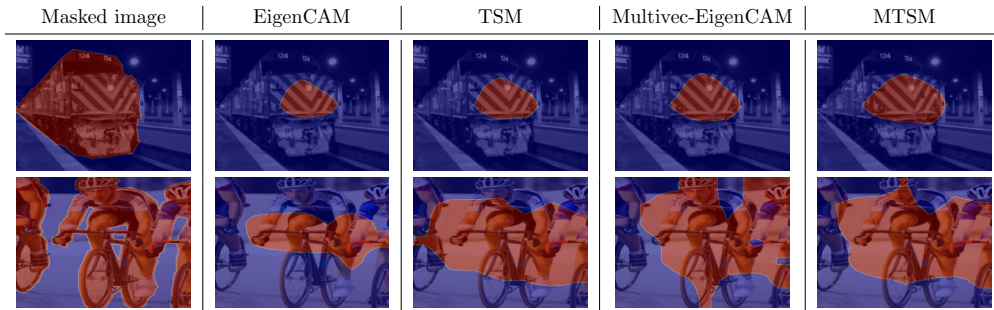


Figure 6: Qualitative comparison of saliency maps extracted using the EigenCAM versus TSM on the VicRegL Resnet50 model, juxtaposed with the segmentation mask from the Pascal VOC dataset. The showcased segmentations based on the saliency maps employ a threshold of 0.5.

Lastly, we compare the saliency maps produced through supervised classification models in Figure 4 and the ones produced through self-supervised models in Figure 5. We notice that the all label-independent saliency map methods are not class specific but the learning task has an impact on the produced map. This is particularly evident on the gymnast image. We notice that for the classification models, the gymnast and the balance beam are highlighted however the self-supervised models adds-in the crowd in the background among the highlighted regions. The reason being, the crowd is in the background and has little importance to the classification model. Yet, for the self-supervised model trained with a form of contrastive loss, the background presents significant information allowing the model to differentiate the image from the rest of the images in the dataset hence minimizing the loss function.

## 7 Conclusion

In this work, we introduce the TSM method, a label-independent CNN explainability method harnessing tensor algebra notably Tucker tensor decomposition to produce high quality and fidelity saliency maps of CNN’s input regions. TSM is a principled method, not restricted to supervised classification CNN models and yet achieves competitive quantitative and qualitative results compared to label-dependent methods. Moreover, compared to the only CNN label-independent method namely EigenCAM, TSM allows for a more accurate estimation of singular vectors and values resulting in more accurate saliency maps. Furthermore, we extend the EigenCAM and TSM method to the Multivec-EigenCAM and MTSM which take profit of all the singular vectors and values further improving the explainability of supervised and self-supervised CNN models. We test all the label-independent methods on various supervised classification CNN models via established metrics and on self-supervised CNN models through an evaluation procedure we propose. When comparing EigenCAM to TSM, our results indicate a 50% improvement in quantitative results on all tested metrics and models. Multivec-EigenCAM and MTSM further improve on the performance of their base methods with varying extents depending on the amount of variance encoded by each singular vector. Our qualitative results showcase that EigenCAM can be misleading when used as an explainability method. This is because it highlights fewer regions of the input in the saliency map compared to our proposed methods which are more reliable since they highlight all the significant regions.

It worth noting that TSM and MTSM come with increased computational costs, requiring approximately  $2.5\times$  more processing time than EigenCAM due to the Tucker tensor decomposition. Despite this complexity, the significant improvements in explainability and the methods’ effectiveness in interpreting self-supervised models justify the additional computational burden. Future work will focus on optimization techniques to reduce execution time, ensuring that these methods remain efficient.

## Acknowledgments

This work received access to the High-Performance Computing (HPC) resources of MesoPSL, financed by the Region Île-de-France and the Equip@Meso project (reference ANR-10-EQPX-29-01) of the Investissements d’avenir program supervised by the Agence nationale pour la recherche.

## References

- Kjersti Aas, Martin Jullum, and Anders Løland. Explaining individual predictions when features are dependent: More accurate approximations to shapley values. *Artificial Intelligence*, 298:103502, 03 2021. doi: 10.1016/j.artint.2021.103502.
- Sebastian Bach, Alexander Binder, Grégoire Montavon, Frederick Klauschen, Klaus-Robert Müller, and Wojciech Samek. On pixel-wise explanations for non-linear classifier decisions by layer-wise relevance propagation. *PLOS ONE*, 10(7):1–46, 07 2015. doi: 10.1371/journal.pone.0130140. URL <https://doi.org/10.1371/journal.pone.0130140>.
- Adrien Bardes, Jean Ponce, and Yann LeCun. VICRegL: Self-supervised learning of local visual features. In S. Koyejo, S. Mohamed, A. Agarwal, D. Belgrave, K. Cho, and A. Oh (eds.), *Advances in Neural Information Processing Systems*, volume 35, pp. 8799–8810. Curran Associates, Inc., 2022.

- 
- Aymene Mohammed Bouayed, Samuel Deslauriers-Gauthier, Mauro Zucchelli, and Rachid Deriche. CNN and diffusion MRI’s 4th degree rotational invariants for Alzheimer’s disease identification. In Nuno Moniz, Paula Branco, Luís Torgo, Nathalie Japkowicz, Michal Wozniak, and Shuo Wang (eds.), *Proceedings of the Fourth International Workshop on Learning with Imbalanced Domains: Theory and Applications*, volume 183 of *Proceedings of Machine Learning Research*, pp. 163–174. PMLR, 23 Sep 2022.
- Fadi Boutros, Marco Huber, Patrick Siebke, Tim Rieber, and Naser Damer. SFace: Privacy-friendly and accurate face recognition using synthetic data. In *IEEE International Joint Conference on Biometrics, IJCB 2022, Abu Dhabi, United Arab Emirates, October 10-13, 2022*, pp. 1–11. IEEE, 2022. doi: 10.1109/IJCB54206.2022.10007961. URL <https://doi.org/10.1109/IJCB54206.2022.10007961>.
- Giuseppe Bove. Methods for the analysis of skew-symmetry in asymmetric multidimensional scaling. In Hermann Locarek-Junge and Claus Weihs (eds.), *Classification as a Tool for Research*, pp. 271–278, Berlin, Heidelberg, 2010. Springer Berlin Heidelberg. ISBN 978-3-642-10745-0.
- Mathilde Caron, Ishan Misra, Julien Mairal, Priya Goyal, Piotr Bojanowski, and Armand Joulin. Unsupervised learning of visual features by contrasting cluster assignments. In H. Larochelle, M. Ranzato, R. Hadsell, M.F. Balcan, and H. Lin (eds.), *Advances in Neural Information Processing Systems*, volume 33, pp. 9912–9924. Curran Associates, Inc., 2020.
- Aditya Chattopadhyay, Anirban Sarkar, Prantik Howlader, and Vineeth N Balasubramanian. Grad-CAM++: Generalized gradient-based visual explanations for deep convolutional networks. In *2018 IEEE Winter Conference on Applications of Computer Vision (WACV)*, pp. 839–847, 2018. doi: 10.1109/WACV.2018.00097.
- Xinlei Chen, Haoqi Fan, Ross Girshick, and Kaiming He. Improved baselines with momentum contrastive learning. *arXiv preprint arXiv:2003.04297*, 2020.
- Lei Cheng, Zhongtao Chen, and Yik-Chung Wu. *Tensor Decomposition: Basics, Algorithms, and Recent Advances*, pp. 1–14. Springer International Publishing, 2023. doi: 10.1007/978-3-031-22438-6\_1.
- Federica Cruciani, Lorenza Brusini, Mauro Zucchelli, Gustavo Retuci Pinheiro, Francesco Setti, Ilaria Boscolo Galazzo, Rachid Deriche, Leticia Rittner, Massimiliano Calabrese, and Gloria Menegaz. Explainable 3D-CNN for Multiple Sclerosis patients stratification. In *ICPR 2020 - 25th International Conference on Pattern Recognition Workshops and Challenges*, pp. 103–114, 2021. doi: 10.1007/978-3-030-68796-0\_8. URL <https://hal.science/hal-02971361>.
- Lieven De Lathauwer, Bart De Moor, and Joos Vandewalle. A multilinear singular value decomposition. *SIAM Journal on Matrix Analysis and Applications*, 21(4):1253–1278, 2000. doi: 10.1137/S0895479896305696.
- Jia Deng, Wei Dong, Richard Socher, Li-Jia Li, Kai Li, and Li Fei-Fei. ImageNet: A large-scale hierarchical image database. In *2009 IEEE Conference on Computer Vision and Pattern Recognition*, pp. 248–255, 2009. doi: 10.1109/CVPR.2009.5206848.
- Saurabh Desai and Harish G. Ramaswamy. Ablation-CAM: Visual explanations for deep convolutional network via gradient-free localization. In *2020 IEEE Winter Conference on Applications of Computer Vision (WACV)*, pp. 972–980, 2020. doi: 10.1109/WACV45572.2020.9093360.
- M. Everingham, L. Van Gool, C. K. I. Williams, J. Winn, and A. Zisserman. The pascal visual object classes (VOC) challenge. *International Journal of Computer Vision*, 88(2):303–338, June 2010.
- Ruigang Fu, Qingyong Hu, Xiaohu Dong, Yulan Guo, Yinghui Gao, and Biao Li. Axiom-based Grad-CAM: Towards accurate visualization and explanation of CNNs. *British Machine Vision Conference*, 2020.
- Kaiming He, Xiangyu Zhang, Shaoqing Ren, and Jian Sun. Deep residual learning for image recognition. In *Proceedings of the IEEE Conference on Computer Vision and Pattern Recognition (CVPR)*, pp. 770–778, 2016.

- 
- T. Ichiishi. *Game Theory for Economic Analysis*. Economic Theory, Econometrics, and Mathematical Economics. Elsevier Science, 1983. ISBN 9780123701800. URL <https://books.google.fr/books?id=zFm7AAAAIAAJ>.
- Paul Jaccard. Etude de la distribution florale dans une portion des Alpes et du Jura. *Bulletin de la Societe Vaudoise des Sciences Naturelles*, 37:547–579, 01 1901. doi: 10.5169/seals-266450.
- Jacob Gildenblat et al. Pytorch library for CAM methods. <https://github.com/jacobgil/pytorch-grad-cam>, 2021.
- Naimul Mefraz Khan, Nabila Abraham, and Marcia Hon. Transfer learning with intelligent training data selection for prediction of Alzheimer’s disease. *IEEE Access*, 7:72726–72735, 2019. doi: 10.1109/ACCESS.2019.2920448.
- Henk A. L. Kiers. Towards a standardized notation and terminology in multiway analysis. *Journal of Chemometrics*, 14(3):105–122, 2000.
- Eunji Kim and Sungzoon Cho. Exposing fake faces through deep neural networks combining content and trace feature extractors. *IEEE Access*, 9:123493–123503, 2021. doi: 10.1109/ACCESS.2021.3110859.
- Daiki Kimura, Subhajit Chaudhury, Minori Narita, Asim Munawar, and Ryuki Tachibana. Adversarial discriminative attention for robust anomaly detection. In *2020 IEEE Winter Conference on Applications of Computer Vision (WACV)*, pp. 2161–2170, 2020. doi: 10.1109/WACV45572.2020.9093428.
- Alexander Kirillov, Eric Mintun, Nikhila Ravi, Hanzi Mao, Chloe Rolland, Laura Gustafson, Tete Xiao, Spencer Whitehead, Alexander C. Berg, Wan-Yen Lo, Piotr Dollar, and Ross Girshick. Segment anything. In *Proceedings of the IEEE/CVF International Conference on Computer Vision (ICCV)*, pp. 4015–4026, October 2023.
- Narine Kokhlikyan, Vivek Miglani, Miguel Martin, Edward Wang, Bilal Alsallakh, Jonathan Reynolds, Alexander Melnikov, Natalia Kliushkina, Carlos Araya, Siqi Yan, and Orion Reblitz-Richardson. Captum: A unified and generic model interpretability library for pytorch, 2020.
- Tamara G. Kolda and Brett W. Bader. Tensor decompositions and applications. *SIAM Review*, 51(3):455–500, 2009. doi: 10.1137/07070111X.
- Alex Krizhevsky, Ilya Sutskever, and Geoffrey E. Hinton. ImageNet classification with deep convolutional neural networks. *Commun. ACM*, 60(6):84–90, May 2017. ISSN 0001-0782. doi: 10.1145/3065386. URL <https://doi.org/10.1145/3065386>.
- Ze Liu, Yutong Lin, Yue Cao, Han Hu, Yixuan Wei, Zheng Zhang, Stephen Lin, and Baining Guo. Swin transformer: Hierarchical vision transformer using shifted windows. In *Proceedings of the IEEE/CVF International Conference on Computer Vision (ICCV)*, pp. 10012–10022, October 2021.
- Zhuang Liu, Hanzi Mao, Chao-Yuan Wu, Christoph Feichtenhofer, Trevor Darrell, and Saining Xie. A ConvNet for the 2020s. In *Proceedings of the IEEE/CVF Conference on Computer Vision and Pattern Recognition (CVPR)*, pp. 11976–11986, 2022.
- Scott M. Lundberg and Su-In Lee. A unified approach to interpreting model predictions. In I. Guyon, U. Von Luxburg, S. Bengio, H. Wallach, R. Fergus, S. Vishwanathan, and R. Garnett (eds.), *Proceedings of the 31st International Conference on Advances in Neural Information Processing Systems*, NeurIPS’17, pp. 4768–4777, Red Hook, NY, USA, 2017. Curran Associates Inc. ISBN 9781510860964.
- Grégoire Montavon, Alexander Binder, Sebastian Lapuschkin, Wojciech Samek, and Klaus-Robert Müller. Layer-wise relevance propagation: An overview. *Lecture Notes in Computer Science (including subseries Lecture Notes in Artificial Intelligence and Lecture Notes in Bioinformatics)*, pp. 193–209, 09 2019. doi: 10.1007/978-3-030-28954-6\_10.



- 
- Mohammed Bany Muhammad and Mohammed Yeasin. Eigen-CAM: Class activation map using principal components. In *2020 International Joint Conference on Neural Networks (IJCNN)*, pp. 1–7, 2020. doi: 10.1109/IJCNN48605.2020.9206626.
- Justin Johnson Nikhil Naik Ramprasaath R. Selvaraju, Karan Desai. Casting your model: Learning to localize improves self-supervised representations. In *CVPR*, 2021.
- Joseph Redmon, Santosh Divvala, Ross Girshick, and Ali Farhadi. You Only Look Once: Unified, real-time object detection. In *Proceedings of the IEEE Conference on Computer Vision and Pattern Recognition (CVPR)*, pp. 779–788, June 2016.
- Marco Tulio Ribeiro, Sameer Singh, and Carlos Guestrin. "why should i trust you?": Explaining the predictions of any classifier. In *Proceedings of the 22nd ACM SIGKDD International Conference on Knowledge Discovery and Data Mining, KDD '16*, pp. 1135–1144, New York, NY, USA, 2016. Association for Computing Machinery. ISBN 9781450342322. doi: 10.1145/2939672.2939778. URL <https://doi.org/10.1145/2939672.2939778>.
- Karl Schulz, Leon Sixt, Federico Tombari, and Tim Landgraf. Restricting the flow: Information bottlenecks for attribution. In *International Conference on Learning Representations*, 2020. URL <https://openreview.net/forum?id=S1xWh1rYwB>.
- Ramprasaath R. Selvaraju, Michael Cogswell, Abhishek Das, Ramakrishna Vedantam, Devi Parikh, and Dhruv Batra. Grad-CAM: Visual explanations from deep networks via gradient-based localization. In *Proceedings of the IEEE International Conference on Computer Vision (ICCV)*, pp. 618–626, Oct 2017.
- Bernard Sheehan and Yousef Saad. Higher Order Orthogonal Iteration of Tensors (HOOI) and its relation to PCA and GLRAM. In *Proceedings of the Seventh SIAM International Conference on Data Mining*, pp. 355–365, 2007. doi: 10.1137/1.9781611972771.32.
- Avanti Shrikumar, Peyton Greenside, and Anshul Kundaje. Learning important features through propagating activation differences. In Doina Precup and Yee Whye Teh (eds.), *Proceedings of the 34th International Conference on Machine Learning*, volume 70 of *Proceedings of Machine Learning Research*, pp. 3145–3153. PMLR, 06–11 Aug 2017.
- Yangyang Shu, Anton van den Hengel, and Lingqiao Liu. Learning common rationale to improve self-supervised representation for fine-grained visual recognition problems. In *Proceedings of the IEEE/CVF Conference on Computer Vision and Pattern Recognition*, pp. 11392–11401, 2023.
- Karen Simonyan and Andrew Zisserman. Very deep convolutional networks for large-scale image recognition. *arXiv preprint arXiv:1409.1556*, 2014.
- Jost Tobias Springenberg, Alexey Dosovitskiy, Thomas Brox, and Martin Riedmiller. Striving for simplicity: The all convolutional net. *arXiv preprint arXiv:1412.6806*, 2015.
- L.N. Trefethen and D. Bau. *Numerical Linear Algebra*. Other Titles in Applied Mathematics. Society for Industrial and Applied Mathematics, 1997. ISBN 9780898713619. URL <https://books.google.fr/books?id=bj-Lu6zjWbEC>.
- Jason Walsh, Alice Othmani, Mayank Jain, and Soumyabrata Dev. Using U-Net network for efficient brain tumor segmentation in MRI images. *Healthcare Analytics*, 2:100098, 2022. ISSN 2772-4425. doi: <https://doi.org/10.1016/j.health.2022.100098>. URL <https://www.sciencedirect.com/science/article/pii/S2772442522000429>.
- Haofan Wang, Zifan Wang, Mengnan Du, Fan Yang, Zijian Zhang, Sirui Ding, Piotr Mardziel, and Xia Hu. Score-CAM: Score-weighted visual explanations for convolutional neural networks. In *Proceedings of the IEEE/CVF Conference on Computer Vision and Pattern Recognition (CVPR) Workshops*, pp. 111–119, June 2020.



- 
- Jure Zbontar, Li Jing, Ishan Misra, Yann LeCun, and Stephane Deny. Barlow Twins: Self-supervised learning via redundancy reduction. In Marina Meila and Tong Zhang (eds.), *Proceedings of the 38th International Conference on Machine Learning*, volume 139 of *Proceedings of Machine Learning Research*, pp. 12310–12320. PMLR, 18–24 Jul 2021.
- Hanwei Zhang, Felipe Torres, Ronan Sircé, Yannis Avrithis, and Stephane Ayache. Opti-cam: Optimizing saliency maps for interpretability. *Computer Vision and Image Understanding*, 248:104101, 2024. ISSN 1077-3142. doi: <https://doi.org/10.1016/j.cviu.2024.104101>.
- Bolei Zhou, Aditya Khosla, Agata Lapedriza, Aude Oliva, and Antonio Torralba. Learning deep features for discriminative localization. In *Proceedings of the IEEE Conference on Computer Vision and Pattern Recognition (CVPR)*, pp. 2921–2929, June 2016.

---

## Supplementary Material

### A Code

Hereafter, we present the implementation of the TSM, Multivec-EigenCAM en MTSM methods proposed in this work using the PyTorch library for Class Activation Map methods, as referenced in [Jacob Gildenblat et al. \(2021\)](#).

```
import torch
import numpy as np
from pytorch_grad_cam.base_cam import BaseCAM
from tensorly.decomposition import Tucker

class TSM(BaseCAM):
    def __init__(self, model, target_layers, use_cuda=False, reshape_transform=None):
        super(TSM, self).__init__(model, target_layers, use_cuda, reshape_transform,
                                   uses_gradients=False)

    def get_cam_image(self, input_tensor, target_layer, target_category, activation_batch,
                      grads, eigen_smooth):
        feature_maps = torch.from_numpy(activation_batch)
        VT = [Tucker(feature_map.numpy(), rank=list(feature_map.shape))[1][0] for
               feature_map in feature_maps]

        VT = torch.from_numpy(np.array(VT))

        VT = VT[:,0].unsqueeze(-1).unsqueeze(-1)
        S = (feature_maps * VT).sum(dim=1)
        return S.abs().numpy()
```

```
import torch
import numpy as np
from pytorch_grad_cam.base_cam import BaseCAM

class MultiVecEigenCam(BaseCAM):
    def __init__(self, model, target_layers, use_cuda=False, reshape_transform=None):
        super().__init__(model=model, target_layers=target_layers, reshape_transform=
                           reshape_transform, uses_gradients=False)

    def get_cam_image(self, input_tensor, target_layer, target_category, activation_batch,
                      grads, eigen_smooth):
        size = (activation_batch.shape[0], activation_batch.shape[-2], activation_batch.shape[-1])

        feature_maps = torch.from_numpy(activation_batch)
        feature_maps = feature_maps.view(
            feature_maps.shape[0], feature_maps.shape[1], -1).permute(0, 2, 1)
        feature_maps = feature_maps - feature_maps.mean(dim=1, keepdim=True)

        _, sigma, VT = torch.linalg.svd(feature_maps, full_matrices=True)
        sigma = sigma.real
        sigma = sigma/sigma.max(dim=1, keepdim=True).values

        cams = []
        for i in range(sigma.shape[1]):
            tmp = VT[:, i].unsqueeze(-1)
            projection = torch.bmm(feature_maps, tmp).view(size)
            weight = sigma[:, i, None, None]
            projection = projection * weight
            cams.append(projection.abs().numpy())

        cam = np.array(cams)
        return cam.mean(0)
```

---

```

import torch
import numpy as np
from pytorch_grad_cam.base_cam import BaseCAM
from tensorly.decomposition import tucker

class MTSM(BaseCAM):
    def __init__(self, model, target_layers, use_cuda=False, reshape_transform=None):
        super(MTSM, self).__init__(model=model, target_layers=target_layers, reshape_transform=
            reshape_transform, uses_gradients=False)

    def get_cam_image(self, input_tensor, target_layer, target_category, activation_batch,
        grads, eigen_smooth):
        feature_maps = torch.from_numpy(activation_batch)
        VT = []
        singular_values = []
        for feature_map in feature_maps:
            t = feature_map.numpy()
            core, factors = tucker(t, rank=list(t.shape))
            VT.append(factors[0])
            singular_values.append(np.linalg.norm(core, axis=(-2,-1), ord='fro'))

        VT = torch.from_numpy(np.array(VT))
        singular_values = torch.from_numpy(np.array(singular_values))
        singular_values /= singular_values.max(dim=1, keepdim=True).values

        saliency_maps = []
        for i in range(singular_values.shape[1]):
            tmp = VT[:,i].unsqueeze(-1).unsqueeze(-1)
            projection = (feature_maps * tmp).mean(dim=1)
            weight = singular_values[:,i].unsqueeze(-1).unsqueeze(-1)
            projection = projection * weight
            saliency_maps.append(projection.detach().abs().numpy())

        S = np.array(saliency_maps)
        S = np.transpose(S, axes=(1,0,2,3))
        S = S.mean(1)
        return S

```

## B Experimental setup

### B.1 Selected layers per model for the CAM inference

In Table 3, we outline the chosen target layers for each examined model. These layers serve as the source from which we extract the feature map tensor for computing the saliency map.

Table 3: Designated layers for saliency map calculation across all tested models and CAM methods in this paper.

Model		Layer
Resnet50	(He et al., 2016)	model.layer4[-1]
ConvNext	(Liu et al., 2022)	model.features
VGG16	(Simonyan & Zisserman, 2014)	model.features
Moco V2	(Chen et al., 2020)	model.layer4[-1]
SWAV	(Caron et al., 2020)	model.layer4[-1]
Barlow Twins	(Zbontar et al., 2021)	model.layer4[-1]
VicRegL Resnet50	(Bardes et al., 2022)	model.layer4[-1]
VicRegL ConvNext	(Bardes et al., 2022)	model.stages[3][2].dwconv

## B.2 Datasets

We evaluate the different saliency map calculation methods in this work on the ImageNet 2012 (Deng et al., 2009) and Pascal VOC (Everingham et al., 2010) datasets. All images of these datasets have been rescaled to a size of  $224 \times 224$ , and the values of the pixels have been normalized to match the preprocessing of the used pre-trained CNNs.

**ImageNet 2012** For this dataset, we use the 50,000 validation images of the ImageNet ILSVRC 2012 dataset (Deng et al., 2009). We mainly use this dataset to calculate the Average Drop, Average Increase and Mean Squared Error metrics.

**Pascal VOC** Owing to the availability of the segmentation masks on the Pascal VOC 2012 challenge dataset (Everingham et al., 2010), we harness this dataset to calculate the mean Intersection over Union metric (Jaccard, 1901).

## B.3 Used libraries

The implementation of the different CAM based saliency map methods is done via the *PyTorch library for CAM methods* (Jacob Gildenblat et al., 2021), the DeepLIFT and DeepSHAP methods are implemented using the Captum Python library (Kokhlikyan et al., 2020) and the LIME method is imported from the official implementation in (Ribeiro et al., 2016).

## B.4 Used classification pretrained models

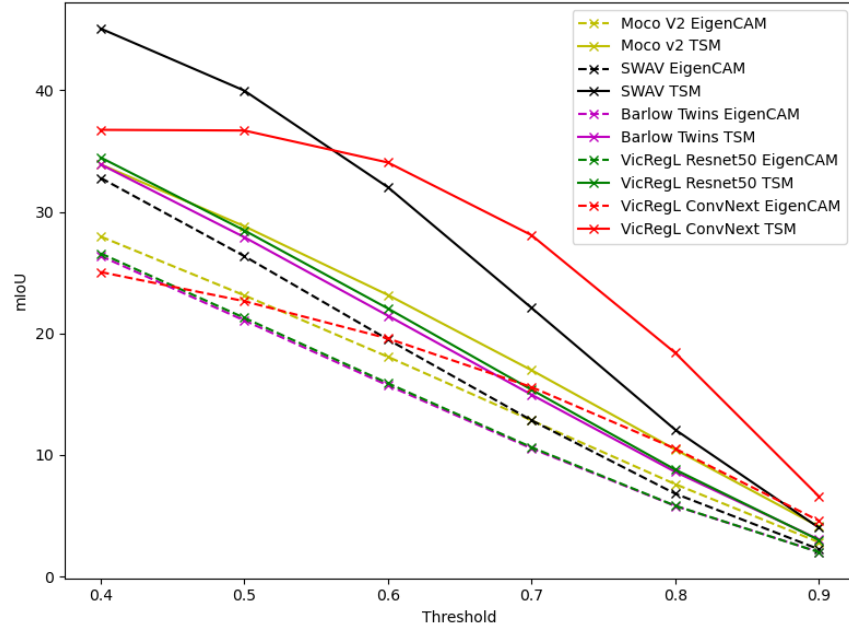
In Table 4, we provide a list of pretrained supervised classification models utilized for computing the Average Drop and Average Increase metrics on the self-supervised models. The primary rationale behind selecting these classification models is their alignment with the backbone model employed in the self-supervised models.

Table 4: Utilized supervised classification models to calculate the metrics of Average Drop and Average Increase on the self-supervised models.

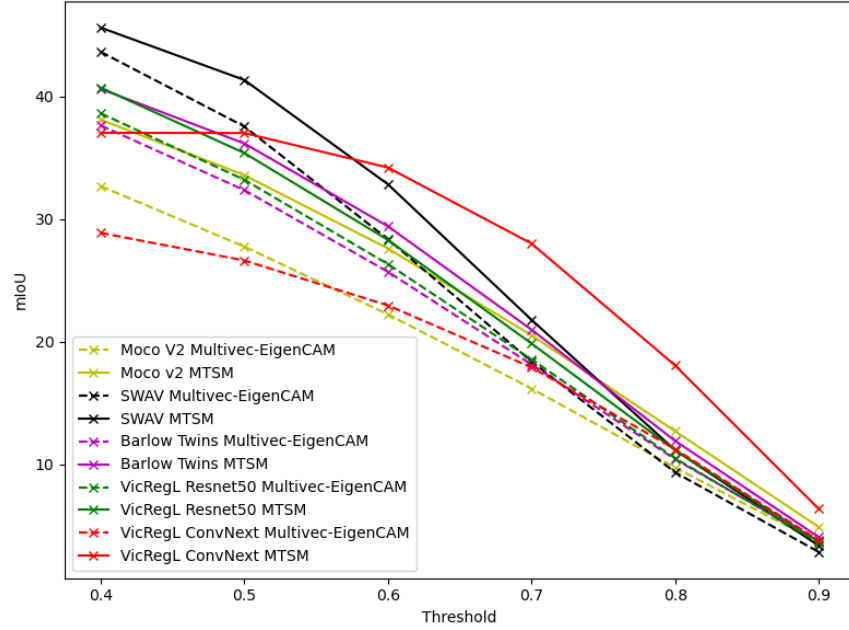
Self-supervised model		Classification model	
Moco V2	(Chen et al., 2020)	Resnet50	(He et al., 2016)
SWAV	(Caron et al., 2020)	Resnet50	(He et al., 2016)
Barlow Twins	(Zbontar et al., 2021)	Resnet50	(He et al., 2016)
VicRegL Resnet50	(Bardes et al., 2022)	Resnet50	(He et al., 2016)
VicRegL ConvNext	(Bardes et al., 2022)	ConvNext	(Liu et al., 2022)

## C Hyperparameter study for the mIoU metric on self-supervised models

In Figure 7, we illustrate our investigation into the threshold hyperparameter employed to binarize saliency maps into segmentation masks and its impact on the mIoU metric. We systematically vary the binarization threshold from 0.4 to 0.9 with a step size of 0.1 and observe the corresponding mIoU values. We exclude threshold values lower than 0.4 as we deem them irrelevant for segmentation. From the observations in Figure 7, it becomes evident that, irrespective of the pretrained self-supervised model, TSM and MTSM yield a more accurate approximation of the segmentation mask than EigenCAM or Multivec-EigenCAM.



(a) Single vector



(b) Multi-vector

Figure 7: On the exploration of the threshold hyperparameter for Class Activation Map (CAM) binarization and its influence on the mIoU metric, solid lines in the plot depict the mIoU values obtained using Tucker decomposition based CAM methods, while dashed lines represent the mIoU values obtained using SVD based CAM methods.

## D Additional supervised models' saliency maps

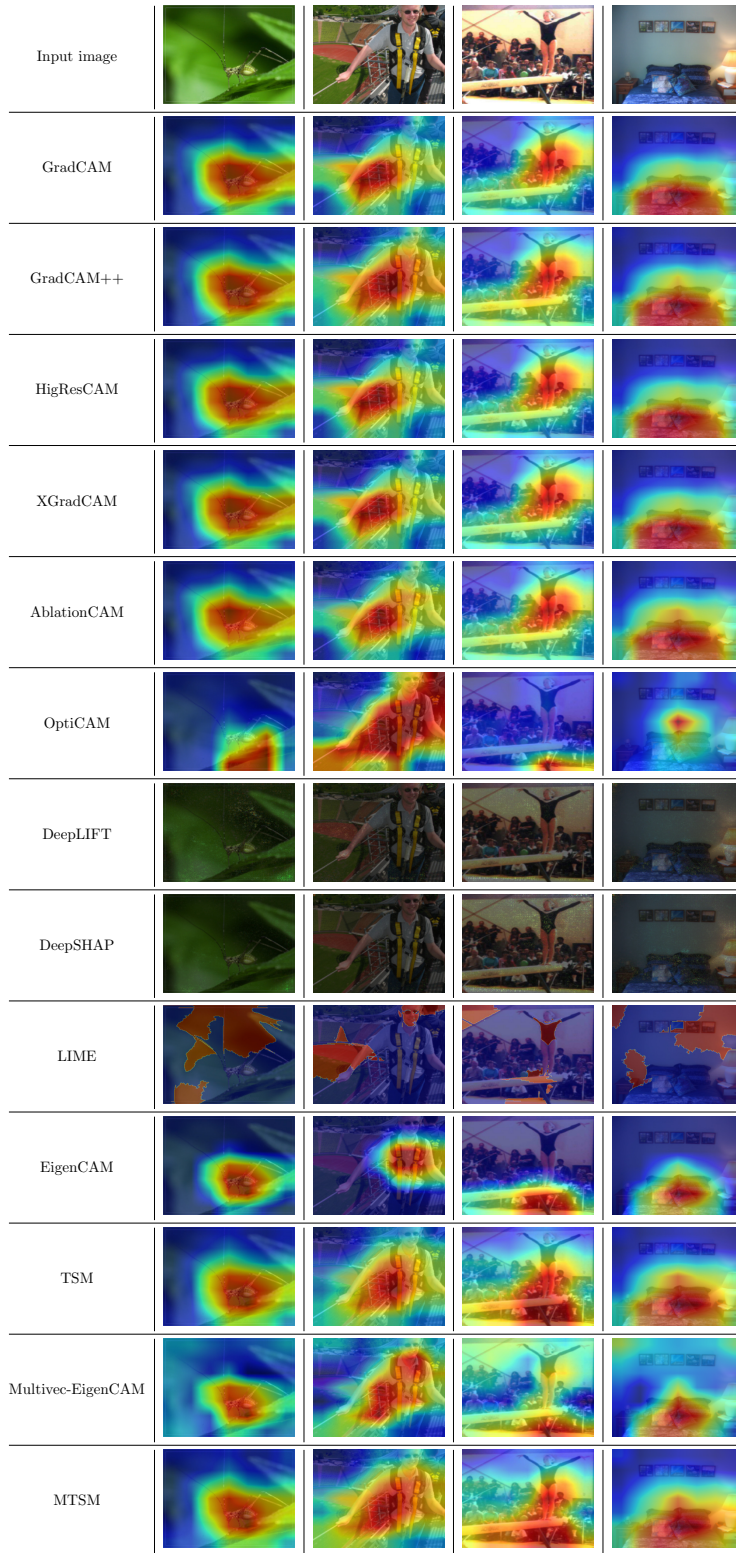


Figure 8: Qualitative comparison of saliency maps calculation methods on the supervised classification Resnet50 model (He et al., 2016) applied to the ImageNet dataset (Deng et al., 2009).







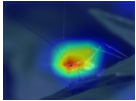
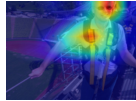
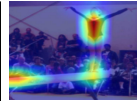
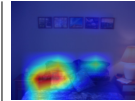
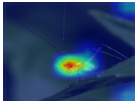
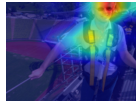
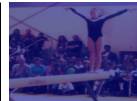

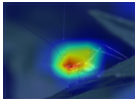
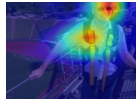
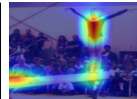
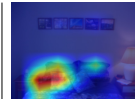
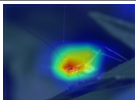
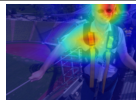

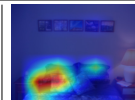
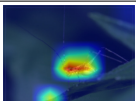
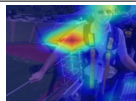

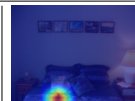
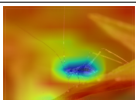
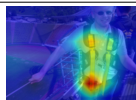

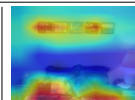
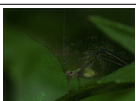

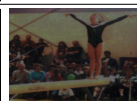
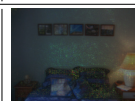


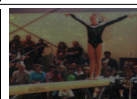
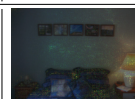


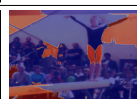

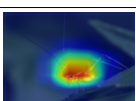


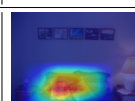
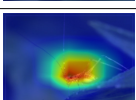

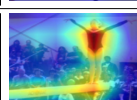
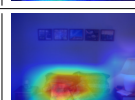
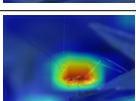


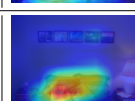
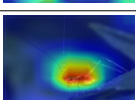


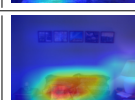
Input image				
GradCAM				
GradCAM++				
HigResCAM				
XGradCAM				
AblationCAM				
OptiCAM				
DeepLIFT				
DeepSHAP				
LIME				
EigenCAM				
TSM				
Multivec-EigenCAM				
MTSM				

Figure 9: Qualitative comparison of saliency maps calculation methods on the supervised classification ConvNext model (Liu et al., 2022) applied to the ImageNet dataset (Deng et al., 2009).





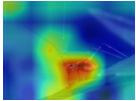
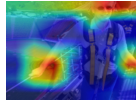
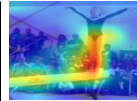
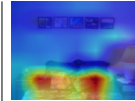
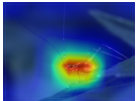
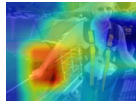
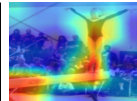
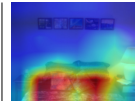
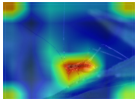
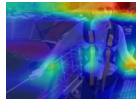
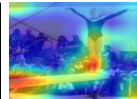
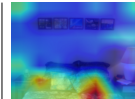
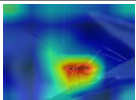
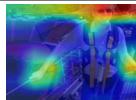
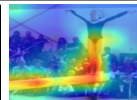
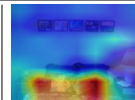
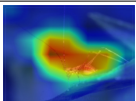
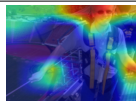
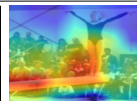
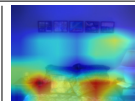
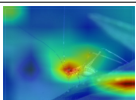
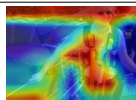

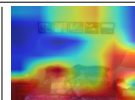
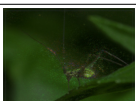

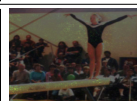
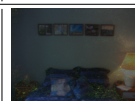


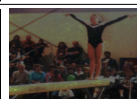
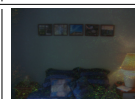


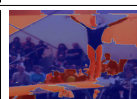

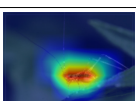

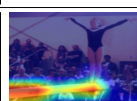
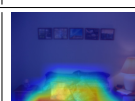
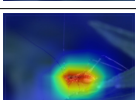

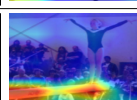
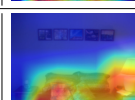
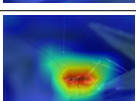

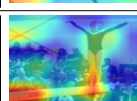
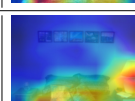
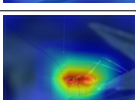


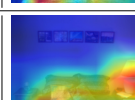
Input image				
GradCAM				
GradCAM++				
HigResCAM				
XGradCAM				
AblationCAM				
OptiCAM				
DeepLIFT				
DeepSHAP				
LIME				
EigenCAM				
TSM				
Multivec-EigenCAM				
MTSM				

Figure 10: Qualitative comparison of saliency maps calculation methods on the supervised classification VGG16 model (Simonyan & Zisserman, 2014) applied to the ImageNet dataset (Deng et al., 2009).

## E Additional self-supervised models' saliency maps

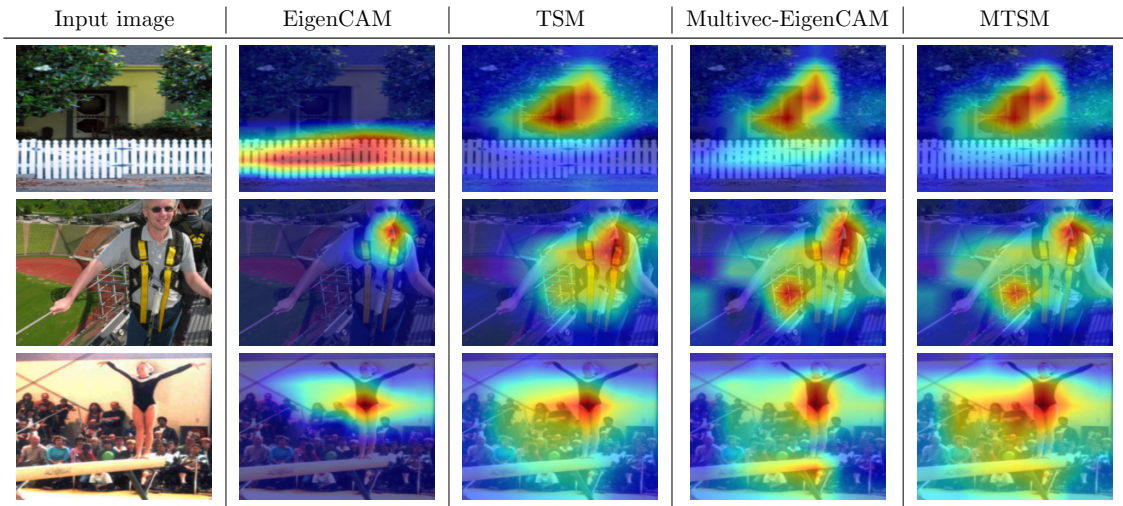


Figure 11: Qualitative comparison of the saliency maps extracted using the EigenCAM method versus the TSM, Multivec-EigenCAM and MTSM methods on the VicRegL Resnet50 model (Bardes et al., 2022) applied to the ImageNet dataset (Deng et al., 2009).

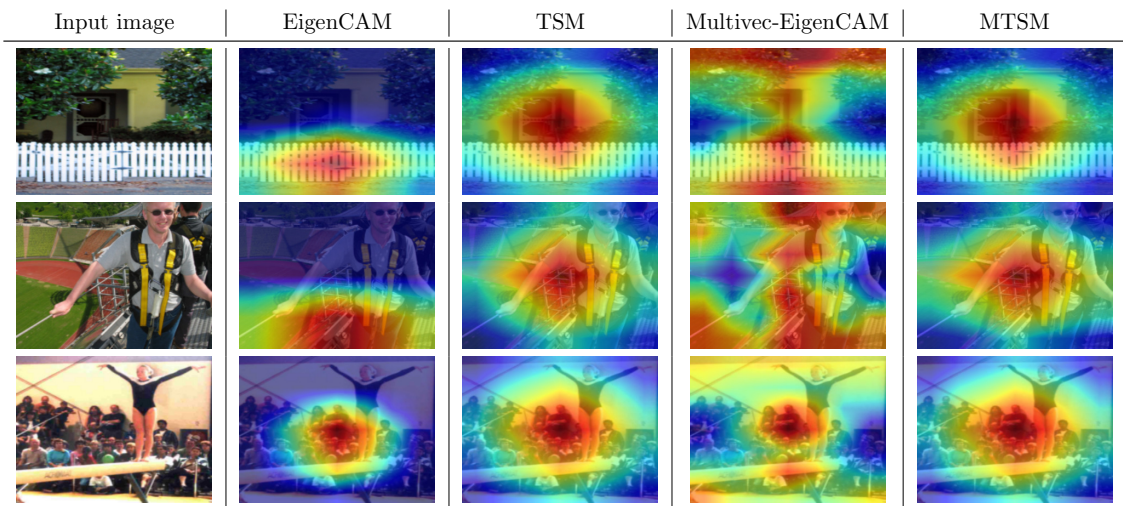


Figure 12: Qualitative comparison of the saliency maps extracted using the EigenCAM method versus the TSM, Multivec-EigenCAM and MTSM methods on the VicRegL ConvNext model (Bardes et al., 2022) applied to the ImageNet dataset (Deng et al., 2009).



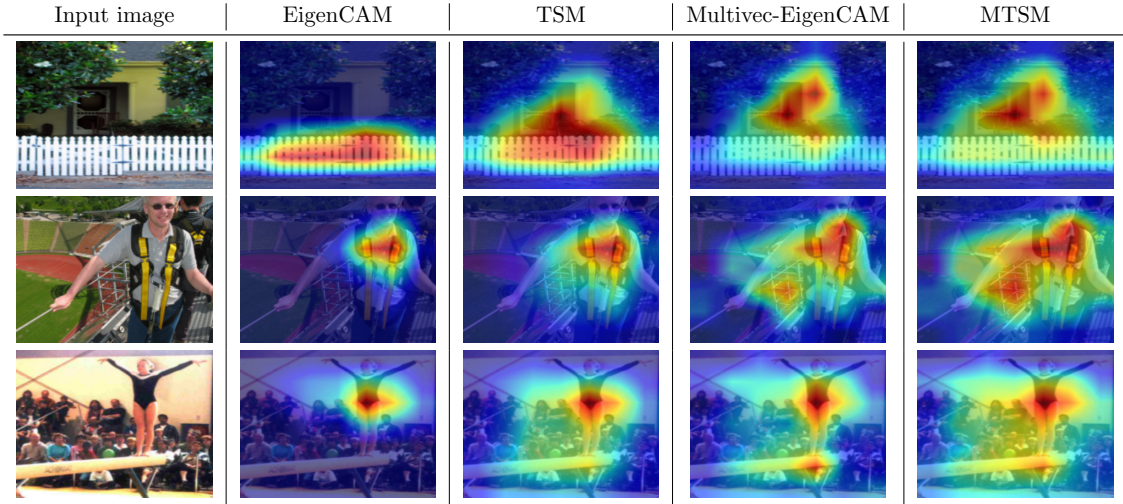


Figure 13: Qualitative comparison of the saliency maps extracted using the EigenCAM method versus the TSM, Multivec-EigenCAM and MTSM methods on the Barlow Twins model (Zbontar et al., 2021) applied to the ImageNet dataset (Deng et al., 2009).

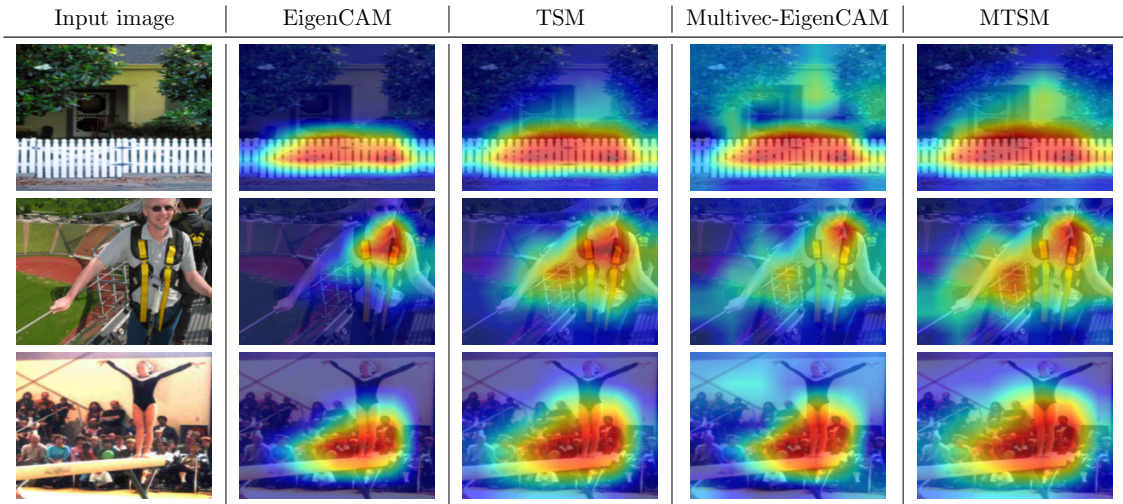


Figure 14: Qualitative comparison of the saliency maps extracted using the EigenCAM method versus the TSM, Multivec-EigenCAM and MTSM methods on the Moco V2 model (Chen et al., 2020) applied to the ImageNet dataset (Deng et al., 2009).

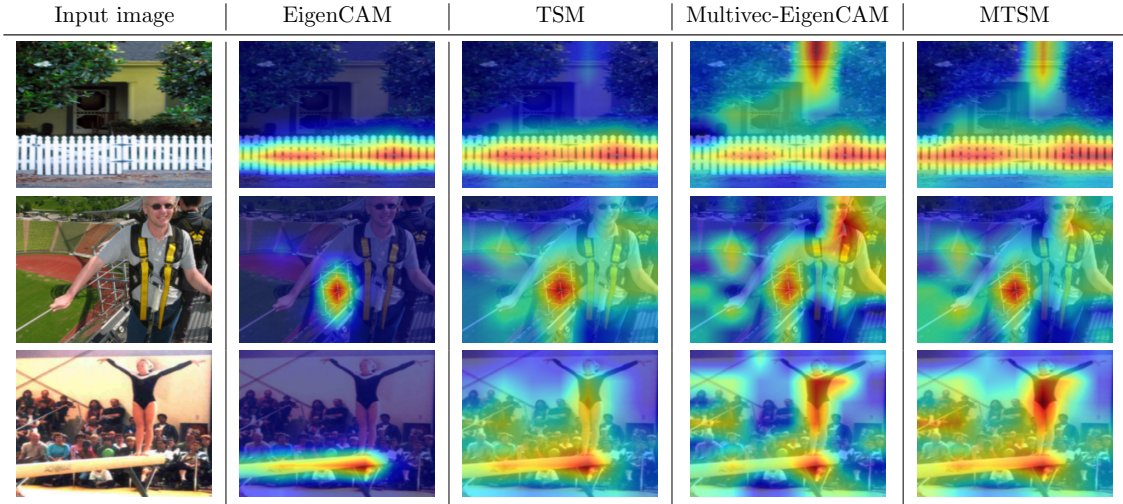


Figure 15: Qualitative comparison of the saliency maps extracted using the EigenCAM method versus the TSM, Multivec-EigenCAM and MTSM methods on the SWAV model (Caron et al., 2020) applied to the ImageNet dataset (Deng et al., 2009).

## F Self-supervised models image segmentation based on CAMs

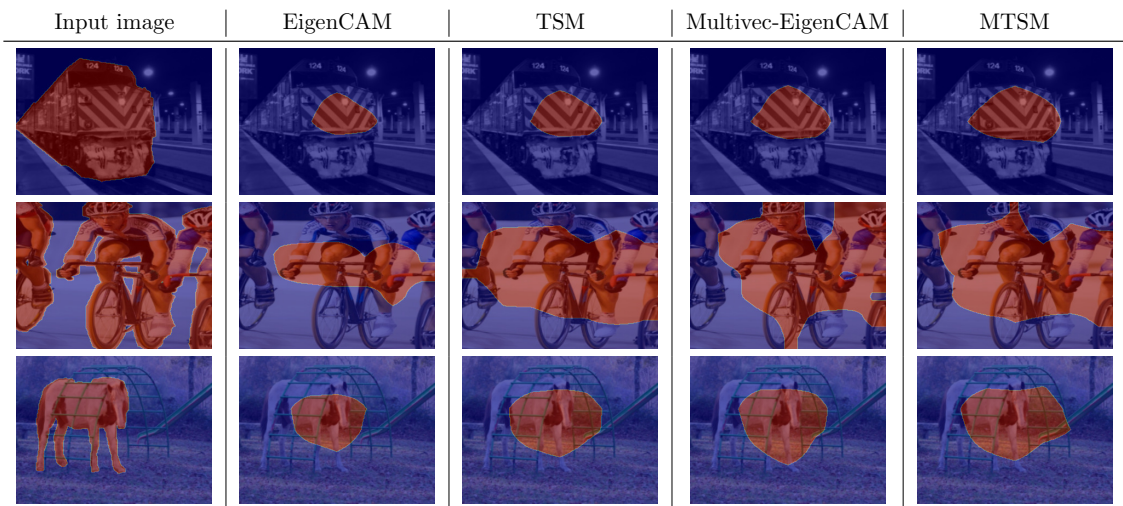


Figure 16: Qualitative comparison of the binarized saliency maps extracted using the EigenCAM method versus the TSM, Multivec-EigenCAM and MTSM methods on the VicRegL Resnet50 model (Bardes et al., 2022), juxtaposed with the segmentation mask from the Pascal VOC dataset (Everingham et al., 2010). The binarization is performed using a 0.5 threshold.

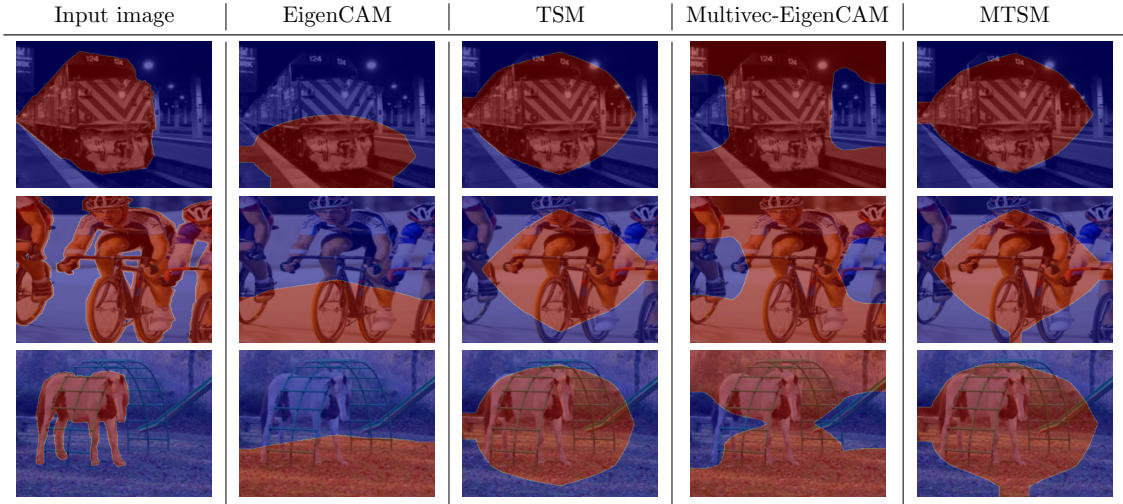


Figure 17: Qualitative comparison of the binarized saliency map extracted using the EigenCAM method versus the TSM, Multivec-EigenCAM and MTSM methods on the VicRegL ConvNext model (Bardes et al., 2022), juxtaposed with the segmentation mask from the Pascal VOC dataset (Everingham et al., 2010). The binarization is performed using a 0.5 threshold.

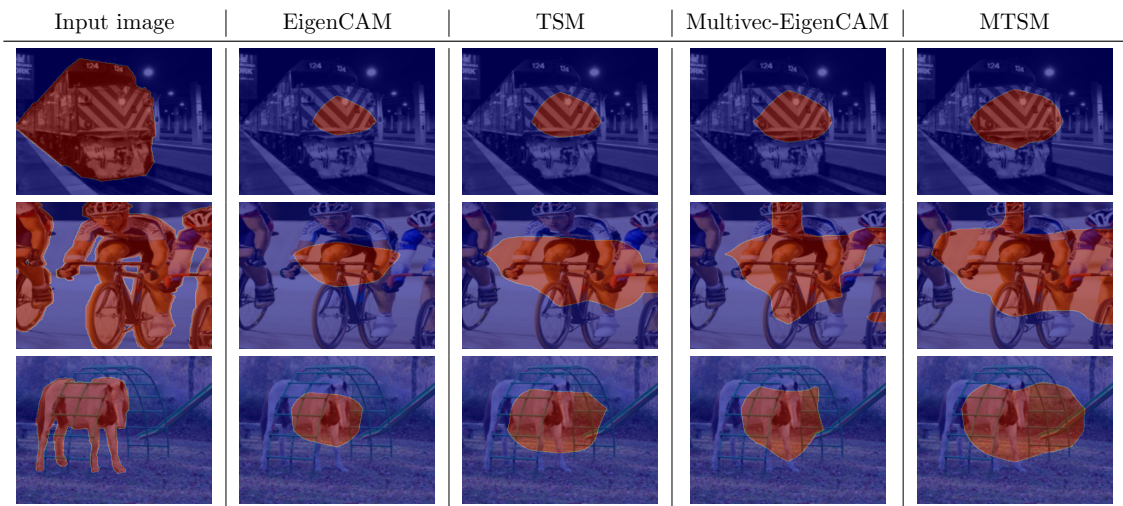


Figure 18: Qualitative comparison of the binarized saliency map extracted using the EigenCAM method versus the TSM, Multivec-EigenCAM and MTSM methods on the Barlow Twins model (Zbontar et al., 2021), juxtaposed with the segmentation mask from the Pascal VOC dataset (Everingham et al., 2010). The binarization is performed using a 0.5 threshold.



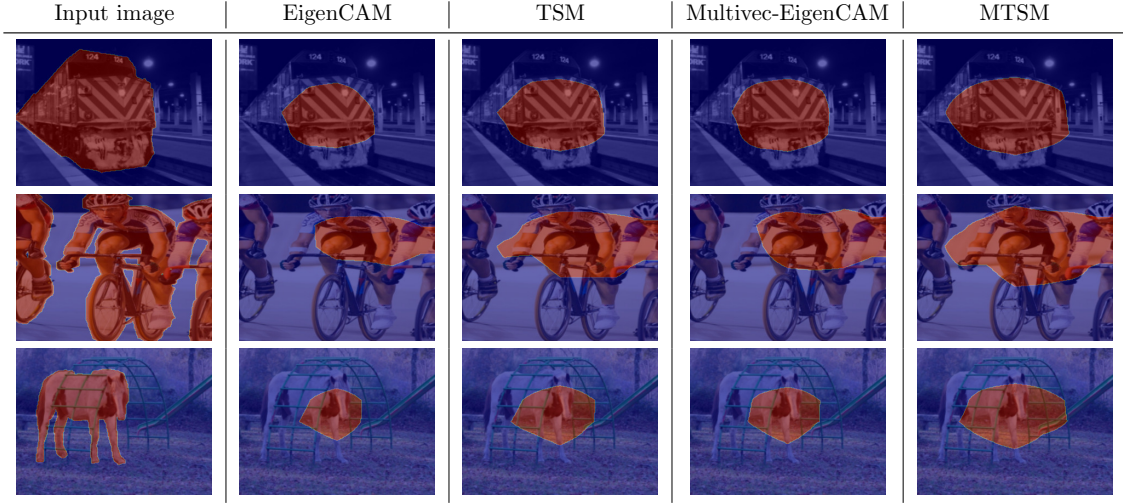


Figure 19: Qualitative comparison of the binarized saliency map extracted using the EigenCAM method versus the TSM, Multivec-EigenCAM and MTSM methods on the Moco V2 model (Chen et al., 2020), juxtaposed with the segmentation mask from the Pascal VOC dataset (Everingham et al., 2010). The binarization is performed using a 0.5 threshold.

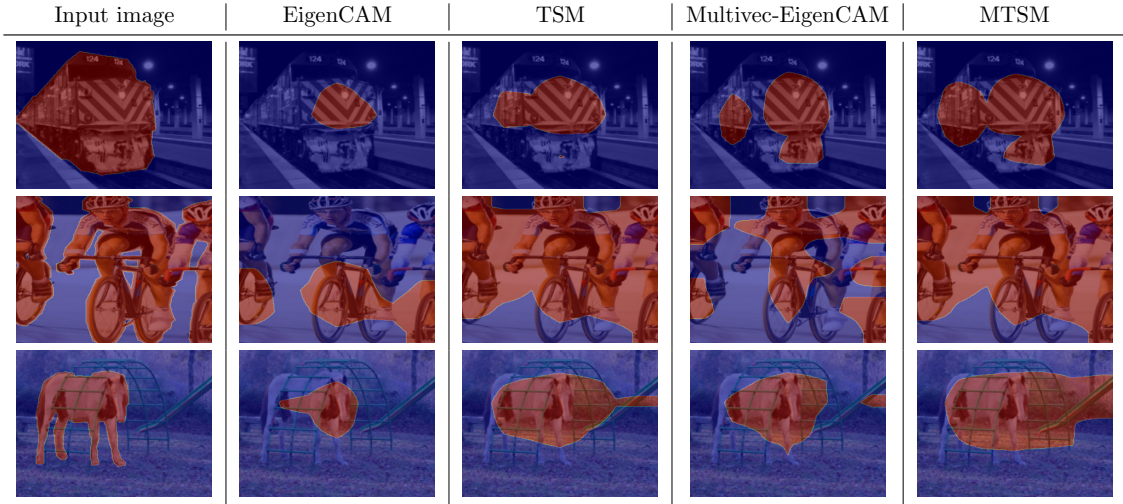


Figure 20: Qualitative comparison of the binarized saliency map extracted using the EigenCAM method versus the TSM, Multivec-EigenCAM and MTSM methods on the SWAV model (Caron et al., 2020), juxtaposed with the segmentation mask from the Pascal VOC dataset (Everingham et al., 2010). The binarization is performed using a 0.5 threshold.